Research Article

Design of novel fluorescent mitochondria-targeted peptides with iron-selective sensing activity

Vincenzo Abbate*†, Olivier Reelfs‡†, Robert C. Hider*, Charareh Pourzand‡[1]

* Institute of Pharmaceutical Science, King's College London, Franklin-Wilkins Building, 150 Stamford Street, London SE19NH, United-Kingdom

‡ Department of Pharmacy and Pharmacology, University of Bath, Claverton Down, Bath BA27AY, United-Kingdom

† Abbate and Reelfs made equal contributions

[1] To whom the correspondence should be addressed: Dr Charareh Pourzand, Department of Pharmacy and Pharmacology, University of Bath, Claverton Down, Bath BA2 7AY, United Kingdom. Email: prscap@bath.ac.uk; Tel: +44 (0) 1225 383590; Fax: +44 (0) 1225 386114

Short Title: Novel fluorescent mitochondria-targeted labile iron sensors

Keywords: Labile iron, iron chelator, iron sensor, SS peptide, cell-penetrating peptide, mitochondria

Abbreviations: ACN, acetonitrile; ATN, anthraniloyl; Boc, di-tert-butyl dicarbonate; CPP(s), cell-penetrating peptide(s); Dap, diaminopropionic acid; DEP, 7-diethylamino-2-oxo-2H-chromen-3-carboxylic acid; DMP, (7-Dimethylamino-2-oxo-2H-chromen-4-yl) acetic acid; DNS, dansyl; EMEM, Earle's modified minimal essential medium; ER, endoplasmic reticulum; $Fe(HQ)_3$, iron(III)-8-hydroxyquinoline; Fe-NTA, Fe-nitrilotriacetate; HBL, Nε-2.3-dihydroxybenzoyllysine; HPO, 3-hydroxypyridin-4-one; HRMS, high resolution mass spectrometry; LI, labile iron; LIP, labile iron pool; MW, molecular weight; ROS, reactive oxygen species; RPA, rhodamine B-[(1,10-phenanthrolin-5-yl)aminocarbonyl] benzylester ; RP-HPLC, reverse phase HPLC; RT, room temperature; SAR, structure-activity relationship; SPPS, solid-phase peptide synthesis; TFA, trifluoroacetic acid; TPP, triphenylphosphonium cations.

Summary Statement: This work introduces novel fluorescent iron chelator-peptides that specifically target mitochondria and sense changes in labile iron levels of the organelle, which is detrimental in oxidative stress and pathological conditions.

ABSTRACT

Mitochondrial labile iron (LI) plays a crucial role in oxidative injuries and pathologies. At present, there is no organelle-specific sensitive iron sensor which can reside exclusively in the mitochondria and reliably monitor levels of LI in this organelle. Here we describe the development of novel fluorescent and highly specific mitochondria iron sensors, using the family of mitochondrial-homing 'SS-peptides' (short cell permeable signal peptides mimicking mitochondrial import sequence) as carriers of highly specific iron chelators for sensitive evaluation of the mitochondrial LI. Microscopic analysis of subcellular localization of a small library of fluorescently labelled SS-like peptides identified dansyl (DNS) as the lead fluorophore for the subsequent synthesis of chimeric iron chelator-peptides of either catechol (compounds **10** and **11**) or hydroxypyridinone (compounds **13** and **14**) type. The iron-sensing ability of these chimeric compounds was confirmed by fluorescent quenching and de-quenching studies both in solution and in cells, with compound **13** exhibiting the highest sensitivity towards iron modulation. The intramolecular fluorophore-chelator distance and the iron affinity both influence probe sensitivity towards iron. These probes represent the first example of highly sensitive mitochondria-directed fluorescent iron chelators with potential to monitor mitochondrial LI levels.

INTRODUCTION

The primary function of mitochondria is to support aerobic respiration and to generate the energy providing substrate, ATP [1]. Given this fundamental role, defects in mitochondrial function have serious physiological consequences. Abnormalities of mitochondrial DNA and oxidative phosphorylation have been identified in several diseases [1, 2].

Recently, mitochondria have been recognized as a principal destination of non protein-bound labile (and chelatable) iron called LI [3]. This redox active mitochondrial labile iron pool (LIP) acts as a catalyst in the formation of reactive oxygen species (ROS) via Fenton chemistry, thereby making these organelles particularly sensitive to oxidative stress seen under certain pathological conditions and leading to cell damage and death [4, 5]. It has been hypothesized that excessive levels of the mitochondrial LIP due to, for instance, defects in iron-sulfur cluster synthesis and function, may result in aging, with disease consequences which have implications particularly in the more common forms of neurodegeneration, namely Friedreich's ataxia, Parkinson's disease and Alzheimer's disease [6-11].

Despite increased deposits of iron having been reported in some of these diseases, monitoring the concentration of mitochondrial LIP both under physiological and pathological conditions has so far proven difficult. Currently there is no mitochondria-specific sensitive iron sensor which can reliably monitor levels of LIP in this organelle. To our knowledge, rhodamine B-[(1,10-phenanthrolin-5-yl)aminocarbonyl] benzylester (RPA) is the only iron-sensitive probe that targets to mitochondria and does so potentiometrically. However the iron-chelating moiety 'phenanthrolin' is not highly specific for iron and in cellular studies, it has been difficult to accurately estimate the level of mitochondrial LIP due to failure to reverse the iron-mediated quenching of RPA by highly specific and potent iron chelators [4]. The development of a selective mitochondrial iron sensor would therefore present an important stepping-stone in the monitoring and adjustment of mitochondrial LIP.

The targeted delivery of biochemical agents to the mitochondria has been shown to enhance both their pharmacological effects and therapeutic window when compared to simple compound delivery [12]. Several pharmaceutical and biotechnological strategies have

been described to address this challenge. For example, conjugation of bioactive drugs, primarily antioxidants, to triphenylphosphonium cations (TPP) allowed selective accumulation into mitochondria, in a membrane potential-driven mechanism both for cell-penetration and for inner mitochondrial membrane accumulation [13-15].

We have focused our attention on the class of small "SS peptides", which selectively target mitochondria [16-19]. Such peptides are amphiphilic, contain alternating aromatic and basic groups, and despite carrying several positive charges, are able to freely penetrate membranes in a non-saturable manner and to rapidly accumulate in the mitochondria [20, 21]. Importantly, they are also able to pass the blood brain barrier. Such mitochondria-directed peptides, as well as some newly-described cationic and lipophilic peptides [22, 23] have been used successfully as carriers of functional molecules (including antioxidants or drugs) to the mitochondria [24-31].

Here, we report the development of selective mitochondrial LI sensors. Using a library of fluorescent mitochondria-targeted amphiphilic tetra- and penta-peptides, we identified a lead compound for the subsequent synthesis of a set of iron chelator-peptides on the basis of selectivity for mitochondrial localization, as determined by fluorescence microscopy. The analysis of the biological trafficking of the compounds highlighted the influence of dye structure on mitochondria localization. A panel of three novel iron chelator-peptides was synthesized which demonstrated sensitive responsiveness to iron, both in cell-free systems and cells. This study has provided a comprehensive investigation of the organelle selectivity and functionality of this novel class of chimeric cell-penetrating peptides (CPPs) and paves the way in the development of selective mitochondrial biosensors for the monitoring of mitochondria-related diseases.

EXPERIMENTAL

Peptide Synthesis

See Supplementary Information for protocols and characterization information.

Analytical

High resolution mass spectrometry (HRMS) was conducted on an Exactive Plus Orbitrap Mass Spectrometer. Analytical reverse phase-HPLC (RP-HPLC) was conducted on a HP1050 HPLC system equipped with an autosampler, a quaternary pump and a Diode-Array Detector. A Kinetex 2.6 μm XB-C18 100A (150 x 2.1 mm) column was employed. The flow rate was 0.2 mL min^{-1} and the eluents were monitored at wavelengths between 214-281 nm. A linear gradient of mobile phase B [acetonitrile (ACN) containing 0.1% trifluoroacetic acid (TFA)] over mobile phase A (0.1% TFA in water) from 0-90% B in 30 min was performed. Data were collected and analyzed using ChemStation software. Semipreparative RP-HPLC was conducted on a Waters SymmetryPrep™ C8, 7 μm, 19 x 300 mm column using water/ACN gradients at a flow rate of 7 mL min^{-1}. The pKa and clog$D_{7.4}$ values were calculated using MarvinView 6.1.3 software. The net charge values were obtained using the calculated pKa values as reference using HySS2009 software.

Cell culture

The human primary foreskin fibroblast (FEK4) cells (kindly provided by Prof. R. M. Tyrrell, University of Bath, UK) were grown as previously described [32], except that phenol red-free culture medium was used. For experiments involving peptide delivery followed by microscopy, cells were seeded on glass coverslips and grown for 2-3 days in

penicillin/streptomycin-free medium in order to reach a confluency of 60-70% on the day of microscopy analysis.

Peptide delivery

Cells grown on coverslips were rinsed twice with serum-free medium, incubated with peptides at a concentration of 1-30 µM for 2 h-overnight at 37 ^{o}C in a humidified chamber and rinsed as before. An organelle-specific marker was then added for 30 min. Following rinsing steps, the coverslips were inverted wet on a glass slide just before live cell microscopy analysis. The peptides were prepared from powder as 50-100 mM stocks in DMSO, kept at 4 ^{o}C and diluted freshly on the day of experiment in warm serum- and phenol red-free Earle's modified minimal essential medium (EMEM) to the concentration required. The organelle-specific markers MitoTracker® Deep Red FM (excitation 644 nm/emission 665 nm), LysoTracker® Deep Red (excitation 647 nm/emission 668 nm) and ER-Tracker™ Red (excitation 587 nm/emission 615 nm) were prepared and used according to manufacturers' recommendations.

Live cell microscopy

Subcellular localization of the DNS- (compounds **3**, **4, 10-11** and **13-14**) and anthraniloyl (ATN)- (compound **2**) labelled peptides was analysed on an Olympus IX51 inverted epifluorescence microscope equipped with a 100 W mercury UV lamp. Cells were imaged with a 40x objective. Images were acquired via an Olympus DP72 digital camera controlled by Olympus cell^P Analysis Image Processing software (Soft Imaging System GmbH, Muenster, Germany). For the subcellular localization of the [(7-Dimethylamino-2-oxo-2H-chromen-4-yl) acetic acid] (DMP)- (compounds **5-7**) and 7-diethylamino-2-oxo-2H-chromen-3-carboxylic acid (DEP)- (compounds **8-9**) labelled peptides, a Zeiss LSM510META inverted confocal microscope equipped with 405 nm blue diode laser, green and red HeNe lasers (543 and 633 nm lines) was used. Cells were imaged with a 63x oil objective. 1-2 µm thick optical slices were collected and processed using the LSM510 software from Zeiss. Cells showing yellow staining, resulting from superimposition of the peptide-specific green signal and the organelle-specific red signal, were qualitatively considered positive for colocalization. The co-occurence in the images, of green and red fluorescent signals above a threshold level was further confirmed by analysis of intensity profiles collected across cells (over a length of ca 30-60µm) using Image Examiner (from Zeiss) and cell^P (from Olympus) Image Processing softwares. The extent of colocalization of each compound with mitochondria, lysosomes or endoplasmic reticulum compartments was also measured quantitatively by Manders' correlation coefficients (MCCs) M1 and M2 using ImageJ software with the JaCoP plug-in [33, 34] from a random selection of image fields. MCCs provide a measure of how much of the signal intensity of a channel occurs in the same location as the other channel. Thus M1 represents the extent of overlap of compound signal (green) with the organelle signal (red), whereas M2 represents the amount of organelle signal overlapping the compound signal. MCCs values range from zero (uncorrelated distributions of two probes with one another) to one (fully correlated distributions of two probes). MCCs were chosen instead of the Pearson's colocalization coefficient as they are particularly well suited when the fluorescent signals distribute to different types of compartments [35].

Fluorescence quenching/dequenching assays

Cell-free system: Quenching experiments were carried out as described previously [36]. ***In-cell studies:*** Responsiveness of fibroblasts FEK4 cells to iron was achieved by loading them with iron(III)-8-hydroxyquinoline [$Fe(HQ)_3$] which was prepared freshly by mixing a solution of ferric chloride (10 mM) in water with 8-hydroxyquinoline (30 mM) in DMSO so

as to obtain a Fe:ligand ratio of 1:3. The complex was then allowed to form for 1 h at 37 ^{o}C before use on cells. Briefly, FEK4 cells were first incubated (or not) overnight, with 30 μM compound **10-11** and **13-14**. The next day, the medium was removed, the cells washed twice with PBS, trypsinized, resuspended in buffer F (10 mM HEPES pH 7.3, 150 mM NaCl) and counted. 10^6 cells were transferred to a thermostated (37 ^{o}C) quartz cuvette and kept in suspension for fluorescence reading with a Kontron spectrofluorimeter (SFM 25, Eching, Germany). Fluorescence was monitored until a stable signal was obtained, upon which iron was added in 0.6-1 μL increments as $Fe(HQ)_3$ complex and fluorescence monitored until a stable signal was obtained before the next addition of iron. The cumulative iron(III) concentrations were: 0, 0.2, 0.4, 0.6, 0.8, 1, 1.2, 1.5, 3, 4.5 and 6 μM. Dequenching of fluorescence was achieved by adding deferiprone as a 100 μM bolus to the iron-loaded cells. PBS, buffer F and the quartz cuvette were all chelex-treated so as to avoid unwanted quenching of compounds' fluorescence.

RESULTS

Design and synthesis of the fluorescent mitochondria-targeted peptides

In the present study, we initially designed and synthesized a series of "SS-like" peptides (see Supplementary data, Figure S1) that were similar in size, but differed in the nature of the fluorophore attached to them, with the view to select a dye that would not interfere with mitochondrial homing of the peptide and with spectroscopic properties that would permit analysis by microscopy. For this purpose, the fluorescent probes chosen were small in size, on the assumption that larger and bulkier fluorophores, such as the commonly used carboxyfluorescein and rhodamine dyes, could perturb the biological behaviour of the relatively small conjugates.

The generic approach for the design of the compound library is illustrated in Figure 1a and the sequences and some physicochemical parameters of the synthesized "SS-like" peptides are presented in Table 1. The peptides were amidated at the C-terminus and incorporated a D-arginine residue in order to increase the peptide stability towards hydrolase enzymes. The compounds were prepared using an orthogonal Fmoc-solid-phase peptide synthesis (SPPS) method, as summarized in Scheme S1 (Supplementary data). This approach was chosen due to its chemical flexibility, efficient peptide preparation and higher safety when compared to the di-tert-butyl dicarbonate (Boc) method, which employs toxic chemicals such as HF. Crude peptides were purified via semi-preparative HPLC and characterized via analytical HPLC and HRMS (see Supplementary data, Table S1).

Compound **1** is the simplest, non-fluorescent compound which was prepared as a control molecule for biophysical evaluation (Table 1). Compound **2** contains an ATN fluorophore, compounds **3** and **4** a DNS fluorophore, compounds **5-7** a DMP fluorophore and compounds **8-9** a DEP fluorophore (Table 1). Since all the fluorescent tetra-peptides possess a predicted charge at neutral pH of approximately +2, we also prepared five-amino acid variants of the DNS, DMP and DEP compounds, possessing a charge of +3 at pH 7.4 in order to evaluate the effect of net charge on their biological trafficking and behaviour (Table 1). Compound **7** displays a DMP fluorophore conjugated to a lysine, rather than a diaminopropionic acid (Dap) residue, in order to assess the influence of the fluorescently labelled amino acid (and the consequent difference in peptide hydrophobicity) on its mitochondria-homing properties.

Intracellular distribution of the fluorescent peptides synthesized

Subcellular distribution of the fluorescent peptides was examined using microscopy on live human skin fibroblast cells in culture and co-labelling with fluorescent commercial markers specific for mitochondria, lysosomes and endoplasmic reticulum (ER), respectively (see Experimental section). Throughout the study, colocalization of the peptides and chelator-peptides to specific organelles was first evaluated qualitatively i) by the occurrence of composite fluorescent yellow signal generated by the co-occurrence of both green and red fluorescent signals above a threshold level and ii) intensity profile comparison as described in Experimental section (see Figures S4 and S5 in Supplementary data). The extent of colocalization of the fluorescent peptides to specific organelles was then investigated quantitatively using ImageJ software with the JaCoP plug-in to determine Manders' correlation coefficients (MCC) M1 (green/red) and M2 (red/green) (See Experimental section and Figure S6).

The overall analysis of the DMP-labelled compounds **5-7** (see example of compound **5** in Figures 2a, D and E; S4, D and S6, M1) and the two DEP-labelled compounds **8-9** (data not shown) unexpectedly showed no detectable mitochondrial localization. Addition of a lysine residue to compound **5** and **9**, forming compound **6** and **8** respectively, in an attempt to improve mitochondria specificity and membrane permeation, did not cause any visible change in cellular distribution (data not shown). None of the DMP- (see example of compound **5** in Figures2a, N and O; S4, N and S6, M1) or the DEP-peptides (data not shown) localized to the ER compartment. However, some colocalization with lysosomes could be observed in a small proportion of cells incubated with compound **5** (Figures 2a, I and J; S4, I and S6, M1) and the DEP-peptides (data not shown). In contrast to the DMP- and DEP-peptides, the DNS-labelled peptides **3-4** were found predominantly in the mitochondrial compartment, with a majority of cells scoring positive for colocalization in that organelle (see example of compound **3** in Figures 2b**,** D and E; S4, D and S6, M1). Addition of a lysine residue to compound **3** forming compound **4** did not detectably improve the mitochondrial distribution (data not shown). With both compounds only some residual lysosomal localisation was detected (see example of compound **3** in Figure 2b**,** I and J, S4, I and S6, M1), but no colocalization with the ER compartment was observed (see example of compound **3** in Figure 2b, N and O, S4, N and S6, M1). The organelle distribution of the ATN-labelled compound **2** was indistinguishable from that of the DNS-peptides (data not shown). Nevertheless, despite fulfilling the criteria of selective mitochondria-homing, compound **2** was not selected for further development due to its spectral properties (see Figure S2, panel a), rendering it impractical to detect microscopically on a routine basis. The DNS-peptides were selected for further investigation.

Biological and functional characterization of the iron chelator-peptides

Our microscopy results with the DNS-peptides prompted the synthesis of compounds **10** and **13-14**, in which the central phenylalanine was replaced by the modified amino acid Nε-2.3-dihydroxybenzoyllysine (HBL) and an ornithine-linked 3-hydroxypyridinone chelator (Mim) respectively, conferring the resultant peptides with the capability to chelate iron (see Figure 1b and Schemes S2 and S3 in Supplementary data). A control peptide - compound **11,** lacking iron chelating capability by methylation of one of the phenol groups was also prepared (see Figure 1b and Scheme S2 in Supplementary data). While compound **11** mimics compound **10** with respect to its biological trafficking (data not shown), it is expected to lack iron binding capacity and provides an iron-inert control to demonstrate the utility of **10** as iron biosensor.

The cellular distribution of compounds **10-11** and **13-14** was assessed by fluorescence microscopy both qualitatively and quantitatively. The overall analysis revealed that in similar fashion to the other DNS-labelled peptides studied –not containing any iron-binding group,

compound **13** localizes predominantly in the mitochondria compartment (see Figures 3, D and E; S5, D and S6, M1). Similar results were obtained with compounds **10** (see Figures S3, S5 and S6, M1 in Supplementary data), **11** and **14** (data not shown).

The responsiveness of compounds **10-11** and **13-14** to iron was monitored using iron-specific fluorescence quenching assays. Fluorescent 3-hydroxypyridin-4-one (HPO) derivatives have been demonstrated to be selectively quenched in the presence of iron(III), iron(II) and copper(II) [36, 37]. However, as the intracellular levels of labile copper(II) are typically 10^{-15} M [38], these molecules are effectively selective for iron under intracellular conditions. A novel lysosome-selective fluorescent iron sensor has also been reported where the fluorescence was found to be sensitive to the presence of iron(III) and selectively quenched by iron(III) in a concentration-dependent manner, both in cell-free systems and in cells in culture [36]. We hypothesized that a similar energy transfer mechanism (see Figure S7 in Supplementary data) would occur with the proposed mitochondria-selective iron sensors **10-11** and **13-14**. Indeed, the incremental addition of iron(III) as Fe-NTA (Fe-nitrilotriacetate) complex to a solution of compound **10** led to the concentration-dependent quenching of its fluorescence, with a maximum quenching effect of ca 60% (Figures 4a and 4e), thereby demonstrating that compound **10** is capable of sensing iron(III) in a cell-free system. In contrast, compound **11** showed no responsiveness when incubated with an iron solution (Figures 4b and 4e), consistent with its lack of capability to bind iron due to the methyl blocking group. These results strongly suggest that the observed decrease in fluorescence intensity in compound **10** is solely due to the formation of a complex between iron and the chelating catechol moiety.

Compounds **13-14** were also investigated as described above to assess the effect on the iron biosensing activity of the intramolecular chelator-fluorophore distance and iron affinity of the chelating group. Compounds **13** and **14** utilise an HPO group as the chelating moiety. With a pFe of around 20, such chelators are several orders of magnitude more powerful than catechols (pFe ~ 15) [39]. Interestingly, in the group of peptides prepared, compound **13** presented the strongest sensitivity towards iron, as revealed by the amplitude of fluorescence quenching (ca 100%) (Figures 4c and 4e), against ca 60% for compound **14** (Figures 4d and 4e) which is similar to the profile of compound **10**.

We assessed the translatability of these findings to FEK4 fibroblast cells, by manipulating the intracellular level of iron(III) using $Fe(HQ)_3$ complex and registering the effect on the fluorescence of the labelled peptide [40] as described in the Experimental section. Addition of as low as 0.2 μM $Fe(HQ)_3$ to cells loaded with compound **13** (Figure 5a) induced a much sharper decrease in fluorescence when compared to cells loaded with compound **10** or **14**. After cumulative addition of 3 μM iron(III), fluorescence quenching of compound **13** reached a plateau at ca 45% of initial fluorescence while quenching of compounds **10** and **14** was less marked (ca 15-20% quenching), albeit significant. As anticipated, when cells were either not loaded with any peptide, or incubated with the "non-chelator" control compound **11**, fluorescence was not affected by addition of iron. In order to ascertain the specificity of the response to LI increase, the cell fluorescence was first followed during incremental addition of iron up to a final concentration of 6 μM (as detailed in the Experimental section). Subsequently, the dequenching of fluorescent signal was monitored after addition of a 100 μM bolus of the potent iron-specific and membrane-permeable chelator deferiprone, with the aim to withdraw iron bound to the tested chelator-peptide localised in the mitochondria. Figure 5b depicts representative fluorescence profiles obtained and reveals that all chelator-peptides are responsive to addition of deferiprone. Furthermore, effective dequenching could be achieved for all three compounds (35-40 min post-addition of deferiprone), demonstrating the iron-dependence of the modulation of fluorescence.

These data, taken together with the mitochondrial-homing properties of these three new compounds successfully demonstrate a proof-of-concept selective delivery to a subcellular organelle of an iron chelator capable of registering mitochondrial LIP.

DISCUSSION

In an attempt to develop highly specific mitochondria-targeted iron sensors, we first investigated the biological trafficking of a series of novel fluorescently labelled SS-like peptides to study the effect of the nature and size of the fluorescent probe as well as the incorporation of additional lysine residue on their mitochondria-targeting ability. As presented in Table 1, compounds **2-9** were essentially fluorescent conjugates of compound **1,** a model SS peptide which is similar to the reported "SS-02" peptide [24], the radiolabelled analogue of which was demonstrated, in cellular studies, to concentrate in mitochondria. Based on its sequence, we anticipated that compound **1** will be targeted to mitochondria and that any biological perturbation observed in compounds **2-9** will be primarily due to the presence of the fluorescent probe. Our cellular distribution data confirmed this prediction. Compounds **2-4** were clearly demonstrated to accumulate in mitochondria, whereas compounds **5-9** were preferentially cytosolic with some minor colocalization with lysosomes. Therefore it appears that the inclusion of ATN or DNS in these model peptides did not interfere with their mitochondria-homing properties, whereas the incorporation of either DMP or DEP is responsible for the loss of specificity of the peptides for the mitochondria, despite their visible uptake by the cells (e.g. Figure 2a B, G and L). Clearly the nature of the fluorophore –even if small in size appears to strongly influence the biological function of a peptide. Our findings with compound **2** are in agreement with the previously reported ATN-conjugated SS peptides [24] demonstrating successful delivery of such fluorescent compounds to the mitochondria. ATN is a small and uncharged fluorescent dye, which probably explains why it does not disrupt the biological activity of the resulting fluorescent peptide when compared to its unlabelled companion (compound **1**). We did not investigate compound **2** in more detail, despite its mitochondria-selective behaviour, due to its weak absorption above 340-350 nm (λ max = 315 nm) and low quantum yield rendering it unpractical to detect with our microscope equipment.

The DNS-conjugated peptides are clearly capable of penetrating membranes. We have investigated some factors that could contribute to the particular mitochondria tropism of the DNS-peptides, guided by the knowledge that the DNS fluorophore is an environment-sensitive dye [41, 42]. Preliminary biophysical results (see Figures S8 and S9 in Supplementary data) on compounds **1** and **3** suggest that the cationic amphipathic peptides change conformation upon interaction with membranes supporting the notion that such cationic amphipathic sequences can penetrate cell-membranes without the need for a transporter or endocytosis [17].

The subcellular distribution data further demonstrated that within each group of peptides bound to a given fluorophore, the addition of a lysine residue did not have a measurable effect on the selectivity for mitochondria.

These findings have also led to the identification of a lead mitochondria-targeted iron chelator. Three DNS-conjugated iron chelator peptides (**10**, **13** and **14**) were selected because they were predicted to colocalise with mitochondria. The entire compound series is highly hydrophilic ($clogD_{7.4} \leq -2$, Table 1) and the introduction of a chelating centre does not appreciably change this value, thus compound **13** has a $clogD_{7.4}$ value of -2.9, presenting multiple positive charges. Such constructs are extremely polar and it will be unlikely that such a molecule will remain located in the inner membrane, rather being localized in the

matrix. Once inside mitochondria, by virtue of its +6 charge it should remain trapped in the aqueous environment, thus sensing the mitochondrial matrix iron levels. The three iron chelators **10**, **13** and **14** have either catechol or HPO as metal ligands. In both cases the ligand has an extremely high-affinity for iron(III), which renders the probes selective for this metal under physiological conditions [43]. By virtue of this extremely high affinity for iron(III), under aerobic conditions these ligands will rapidly autoxidize iron(II) to generate the stable iron(III) complex [44]. Thus all three iron chelators **10**, **13** and **14** sense both iron(III) and iron(II) in cell-free systems and in cells. Amongst these three iron chelator peptides, the HPO-containing compound **13** displayed the highest sensitivity to iron, presumably due to its higher affinity for iron(III) [39]. The lower sensitivity of compound **14** compared to compound **13** may be due to the longer distance between the fluorophore and the iron chelating moiety, resulting in a less efficient energy transfer between those groups upon iron binding. Interestingly the maximum amplitude of iron-specific quenching attained for compounds **13**, **10** and **14** in cell-free systems (i.e. 100, 60 and 60%, respectively) (see Figure 4e) were higher than those typically obtained in cells (i.e. 45, 20 and 15%, respectively). This is likely to be due to the partial quenching of fluorescence during their incubation in cells, prior to the addition of $Fe(HQ)_3$, thereby leading to an apparent lower sensitivity. Nevertheless the order of sensitivity to iron (i.e. in decreasing order of sensitivity **13** > **10** ~ **14**) was preserved both in the cell-free system and in FEK4 cells, therefore validating the cell-free approach to predict sensitivity of this class of compounds in cells. Experiments are currently under way which aim at using the above quenching data to determine the mitochondrial LI in various cell types and conditions, as well as possible effects of these compounds on mitochondrial functions.

In conclusion, compound **13** is the most promising candidate mitochondrial LI sensor of the three compounds we have synthesized. With no adequate mitochondria-specific iron sensors available, our compounds are expected to be of significant value to both biological and pre-clinical research in the field of iron- and mitochondria-related oxidative injuries and pathologies. The use of this mitochondria-targeted iron sensor in physiological and pathological conditions characterized by iron-overload in mitochondria is a long-term objective currently under investigation in our laboratory.

AUTHOR CONTRIBUTIONS

V.A., O.R., R.C.H. and C.P. conceived and designed the research. V.A. and O.R. performed the experiments. V.A., O.R., R.C.H. and C.P. analysed the data. V.A. and O.R. wrote the paper with input from R.C.H. and C.P.

ACKNOWLEDGMENTS

We are grateful to Tobias Krams for the Mass Spectrometry analyses and to Dr Tam Bui for help and support for CD spectroscopy. We thank Prof. Rex Tyrrell for the gift of FEK4 cells. We are also grateful to Prof. David Tosh for allowing us to use his epifluorescence microscope, to Dr Adrian Rogers (Microscopy and Analysis Suite, University of Bath), Dr Mark Jepson and Mr Alan Leard (Wolfson Bioimaging Facility, University of Bristol) for expert help with confocal microscopy.

FUNDING

This work was funded by Biotechnology and Biological Sciences Research Council (BBSRC, Grant no BB/J005223/1).

REFERENCES

1 Schapira, A. H. V. (2006) Mitochondrial disease. Lancet **368**, 70-82.

2 Vafai, S. B. and Mootha, V. K. (2012) Mitochondrial disorders as windows into an ancient organelle. Nature **491**, 374-383.

3 Levi, S. and Rovida, E. (2009) The role of iron in mitochondrial function. Biochim Biophys Acta **1790**, 629-636.

4 Cabantchik, Z. I. (2014) Labile iron in cells and body fluids. Physiology, pathology and pharmacology. Front. Pharmacol. **5**, 1-10.

5 Winterbourn, C. C. (2008) Reconciling the chemistry and biology of reactive oxygen species. Nat Chem Biol. **4,** 278-86.

6 Allen, G. F. G., Toth, R., James, J. and Ganley, I. G. (2013) Loss of iron triggers PINK1/Parkin-independent mitophagy. EMBO. Rep. **14**, 1127-1135.

7 Gille, G. and Reichmann, H. (2011) Iron-dependent functions of mitochondria—relation to neurodegeneration . J. Neural. Transm. **118**, 349-359.

8 Huang, M. L.-H., Becker, E. M., Whitnall, M., Rahmanto, Y. S., Ponka P. and Richardson, D. R. (2009) Elucidation of the mechanism of mitochondrial iron loading in Friedreich's ataxia by analysis of a mouse mutant. Proc. Natl. Acad. Sci. U.S.A. **106**, 16381-16386.

9 Isaya, G. (2014) Mitochondrial iron-sulfur cluster dysfunction in neurodegenerative disease. Front. Pharmacol. **5**, 1-7.

10 Knight, S. A. B., Sepuri, N. B. V., Pain, D. and Dancis, A. (1998) Mt-Hsp70 homolog, Ssc2p, required for maturation of yeast frataxin and mitochondrial iron homeostasis. J. Biol. Chem. **273**, 18389-18393.

11 Whitnall, M., Rahmanto, Y. S., Huang, M. L.-H., Saletta, F., Lok, H. C., Gutierrez, L., Lazaro, F. J., Fleming, A. J., St. Pierre, T. G., Mikhael, M. R., Ponka, P. and Richardson, D. R. (2012) Identification of nonferritin mitochondrial iron deposits in a mouse model of Friedreich ataxia . Proc. Natl. Acad. Sci. U.S.A. **109**, 20590-20595.

12 Murphy, M. P. and Smith, R. A. J. (2007) Targeting antioxidants to mitochondria by conjugation to lipophilic cations . Annu. Rev. Pharmacol. Toxicol. **47**, 629-656.

13 Boddapati, S. V., D'Souza, G. G. M., Erdogan, S., Torchilin, V. P. and Weissig, V. (2008) Organelle-targeted nanocarriers: Specific delivery of liposomal ceramide to mitochondria enhances its cytotoxicity in vitro and in vivo. Nano. Lett. **8**, 2559-2563.

14 Kelso, G. F., Porteous, C. M., Coulter, C. V., Hughes, G., Porteous, W. K., Ledgerwood, E. C., Smith, R. A. J. and Murphy, M. P. (2001) Selective targeting of a redox-active ubiquinone to mitochondria within cells - Antioxidant and antiapoptotic properties. J. Biol. Chem. **276**, 4588-4596.

15 Murphy, M.P. (2008) Targeting lipophilic cations to mitochondria . Biochim. Biophys. Acta-Bioenergetics **1777**, 1028-1031.

16 Rocha, M., Hernandez-Mijares, A., Garcia-Malpartida, K., Banuls, C., Bellod, L. and Victor, V.M. (2010) Mitochondria-Targeted Antioxidant Peptides. Curr. Pharm. Des. **16**, 3124-3131.

17 Szeto, H. H. (2008) Development of Mitochondria-targeted Aromatic-cationic Peptides for Neurodegenerative Diseases. Ann. N. Y. Acad. Sci. **1147**, 112-121.

18 Szeto, H. H. and Schiller, P. W. (2011) Novel therapies targeting inner mitochondrial membrane-from discovery to clinical development . Pharm. Res. **28**, 2669-2679.

19 Zhao, K., Luo, G. X., Zhao, G. M., Schiller, P. W. and Szeto, H. H. (2003) Transcellular transport of a highly polar 3+net charge opioid tetrapeptide. J. Pharmacol. Exp. Ther. **304**, 425-432.

20 Berezowska, I., Chung, N. N., Lemieux, C., Zelent, B., Szeto, H. H. and Schiller, P. W. (2003) Highly potent fluorescent analogues of the opioid peptide [Dmt(1)]DALDA. Peptides **24**, 1195-1200.

21 Zhao, G. M., Qian, X., Schiller, P. W. and Szeto, H. H. (2003) Comparison of [Dmt1]DALDA and DAMGO in Binding and G Protein Activation at μ, δ, and κ Opioid Receptors. J. Pharmacol. Exp. Ther. **307**, 947-954.

22 Horton, K. L., Stewart, K. M., Fonseca, S. B., Guo, Q. and Kelley, S. O. (2008) Mitochondria-penetrating peptides. Chem. Biol. **15**, 375-382.

23 Yousif, L. F., Stewart, K. M., Horton, K. L. and Kelley, S. O. (2009) Mitochondria-Penetrating Peptides: Sequence Effects and Model Cargo Transport. Chembiochem. **10**, 2081-2088.

24 Zhao, K., Zhao, G. M., Wu, D., Soong, Y., Birk, A. V., Schiller, P. W. and Szeto, H. H. (2004) Cell-permeable peptide antioxidants targeted to inner mitochondrial membrane inhibit mitochondrial swelling, oxidative cell death, and reperfusion injury. J. Biol. Chem. **279**, 34682-34690.

25 Song, W., Shin, J., Lee, J., Kim, H., Oh, D., Edelberg, J. M., Wong, S. C., Szeto, H. and Hong, M. K. (2005) A potent opiate agonist protects against myocardial stunning during myocardial ischemia and reperfusion in rats. Coron. Artery Dis. **16**, 407-410.

26 Wu, D., Soong, Y., Zhao, G. M. and Szeto, H. H. (2002) A highly potent peptide analgesic that protects against ischemia-reperfusion-induced myocardial stunning. Am. J. Physiol-Heart Circ. Physiol. **283**, H783-H791.

27 Petri, S., Kiaei, M., Damiano, M., Hiller, A., Wille, E., Manfredi, G., Calingasan, N. Y., Szeto, H. H. and Beal, M. F. (2006) Cell-permeable peptide antioxidants as a novel therapeutic approach in a mouse model of amyotrophic lateral sclerosis. J. Neurochem. **98**, 1141-1148.

28 Yang, L., Zhao, K., Calingasan, N. Y., Luo, G., Szeto, H. H., Beal and M. F. (2009) Mitochondria targeted peptides protect against 1-methyl-4-phenyl-1,2,3,6-tetrahydropyridine neurotoxicity. Antioxid. Redox. Signal. **11**, 2095-2104.

29 Zhao, K., Luo, G. X., Giannelli, S. and Szeto, H. H. (2005) Mitochondria-targeted peptide prevents mitochondrial depolarization and apoptosis induced by tert-butyl hydroperoxide in neuronal cell lines. Biochem. Pharmacol. **70**, 1796-1806.

30 Lei, E. K., Pereira, M. P. and Kelley, S. O. (2013) Tuning the Intracellular Bacterial Targeting of Peptidic Vectors. Angew. Chem. Int. Ed. Engl. **52**, 9660-9663.

31 Pereira, M. P. and Kelley, S. O. (2011) Maximizing the Therapeutic Window of an Antimicrobial Drug by Imparting Mitochondrial Sequestration in Human Cells. J. Am. Chem. Soc. **133**, 3260-3263.

32 Tyrrell, R. M. and Pidoux, M. (1986) Quantitative Differences in Host-Cell Reactivation of Ultraviolet-Damaged Virus in Human-Skin Fibroblasts and Epidermal-Keratinocytes Cultured from the Same Foreskin Biopsy. Cancer Res. **46**, 2665-2669.

33 Bolte, S. and Cordelières, F.P. (2006) A guided tour into subcellular colocalization analysis in light microscopy. J. Microsc. **224**, 213-232.

34 Manders, E.M.M., Verbeek, F.J. and Aten, J.A. (1993) Measurement of co-localization of objects in dual-color confocal images. J. Microsc. **169**, 375–382.

35 Dunn, K. W., Kamocka, M. M. and McDonald, J. H. (2011) A practical guide to evaluating colocalization in biological microscopy. Am. J. Physiol. Cell Physiol. **300**, C723-742.

36 Fakih, S., Podinovskaia, M., Kong, X., Collins, H. L., Schaible, U. E. and Hider, R.C. (2008) Targeting the Lysosome: Fluorescent Iron(III) Chelators To Selectively Monitor Endosomal/Lysosomal Labile Iron Pools. J. Med. Chem. **51**, 4539-4552.
37 Luo, W., Ma, Y. M., Quinn, P. J., Hider, R. C. and Liu, Z.D. (2004) Design, synthesis and properties of novel iron(III)-specific fluorescent probes. J. Pharm. Pharmacol. **56**, 529-536.
38 Hider, R. C. and Kong, X. (2013) Iron speciation in the cytosol: an overview. Dalton Trans. **42**, 3220-3229.
39 Liu, Z. D. and Hider, R. C. (2002) Design of iron chelators with therapeutic application. Coord. Chem. Rev. **232**, 151-171.
40 Ma, Y. M., De Groot, H., Liu, Z. D., Hider, R. C. and Petrat, F. (2006) Chelation and determination of labile iron in primary hepatocytes by pyridinone fluorescent probes. Biochem. J. **395**, 49-55.
41 Baker, J. G., Middleton, R., Adams, L., May, L. T., Briddon, S. J., Kellam, B. and Hill, S. J. (2010) Influence of fluorophore and linker composition on the pharmacology of fluorescent adenosine A(1) receptor ligands . Br. J. Pharmacol. **159**, 772-786.
42 Hohsaka, T., Muranaka, N., Komiyama, C., Matsui, K., Takaura, S., Abe, R., Murakami, H. and Sisido, M. (2004) Position-specific incorporation of dansylated non-natural amino acids into streptavidin by using a four-base codon. FEBS. Lett. **560**, 173-177.
43 Zhou, T., Ma, Y., Kong, X. and Hider, R.C. (2012) Design of iron chelators with therapeutic application. Dalton Trans. **41**, 6371-6389.
44 Ma, Y., Abbate, V. and Hider, R.C. (2015) Iron-sensitive fluorescent probes: monitoring intracellular iron pools. Metallomics. **7**, 212-222.

FIGURE LEGENDS

Figure 1: (**a**) Schematic representation of the design of a library of fluorescent "SS-like" peptides. (**b**) Chemical structures of chimeric compounds **10**, **11**, **13** and **14.**

Figure 2: Representative microscopy images of subcellular localization studies of H-F-r-F-Dap(DMP)-NH_2 (compound **5**) (**a**) and H-F-r-F-Dap(DNS)-NH_2 (compound **3**) **(b)** in FEK4 cells with MitoTracker Deep Red-labelled mitochondria (**A-E**), LysoTracker Deep Red-labelled lysosomes (**F-J**) and ER-Tracker Red-labelled ER (**K-O**). Following incubation with the labelled peptide, cells were treated with 1 μM MitoTracker, 100 nM LysoTracker or 100 nM ER-Tracker for 30 min, rinsed and analysed by microscopy. Fluorescence data were collected and analysed as described in Experimental section. Green (**B, G, L**) and red (**C, H, M**) fluorescence data were merged together (**D, I, N**) to identify colocalization in yellow. Inserts (**E, J, O**) are representative of a magnified region from the merged picture. Phase contrast images (**A, F, K**) corresponding to the fluorescence data are also shown.

Figure 3: Representative microscopy images of subcellular localization studies of DNS-labelled peptide H-F-r-Mim-Dap(DNS)-NH_2 (compound **13**) with mitochondrial (**A-E**), lysosomal (**F-J**) and ER (**K-O**) compartments, performed as described in Experimental section.

Figure 4: Fluorescence intensity profiles as a function of increasing concentrations (0-5 μM range) of iron(III) for compounds **10** (**a**), **11** (**b**), **13** (**c**) and **14** (**d**). Plot of percentage of

fluorescence quenching (mean +/- STD of three independent observations) as a function of increasing iron(III) concentrations (**e**).

Figure 5: Fluorescence quenching and dequenching of compounds **10**, **11**, **13** and **14** in FEK4 cells in response to the manipulation of cellular levels of iron. Cells incubated (or not) with peptide were loaded with iron(III) in the form of $Fe(HQ)_3$ as described in Experimental section and then treated with a bolus of 100 μM of the iron-specific chelator deferiprone. A representative experiment is depicted for each compound. Plots of fluorescence as a function of total iron(III) concentration added (**a**) and as a function of time (**b**).

Table 1: Sequence and physicochemical properties of compounds **1**-**9**.

Compound	Sequence [1]	MW	pKa values (calculated) [2]	clogD 7.4 [2]	Net charge (pH 7.4) [3]
1	H-F-r-F-Dap-NH_2	553.31	7.54; 11.67; 8.09	-5.4	+2.3
2	H-F-r-F-Dap(ATN)-NH_2	672.78	7.68; 12.12; 2.70	-3.1	+ 1.7
3	H-F-r-F-Dap(DNS)-NH_2	786.94	7.68; 12.00; 9.90; 4.63	-5.2	+ 1.7
4	H-F-r-F-K-Dap(DNS)-NH_2	915.11	7.68; 11.94; 10.35; 9.72; 4.63	-1.9	+ 2.7
5	H-F-r-F-Dap(DMP)-NH_2	782.89	7.68; 11.58; 3.36	-6.5	+ 1.7
6	H-F-r-F-K-Dap(DMP)-NH_2	911.06	7.68; 11.53; 10.18; 3.36	-3.3	+ 2.7
7	H-F-r-F-K-(DMP)-NH_2	824.97	7.68; 11.70; 3.36	-2.2	+ 1.7
8	H-F-r-F-K-Dap(DEP)-NH_2	925.09	7.68; 11.51; 10.18; 4.16	-5.7	+ 2.7
9	H-F-r-F-Dap(DEP)-NH_2	796.91	7.68; 11.55; 4.16	-2.4	+ 1.7

[1] Fluorophore indicated in parentheses. L-amino acids in capital letters; D-amino acids in lower letters. All the peptides present C-amidation.
[2] The pKa and $clogD_{7.4}$ values were calculated using MarvinView 6.1.3.
[3] The net charge values were obtained using the calculated pKa values as reference using HySS2009.

FIG. 1

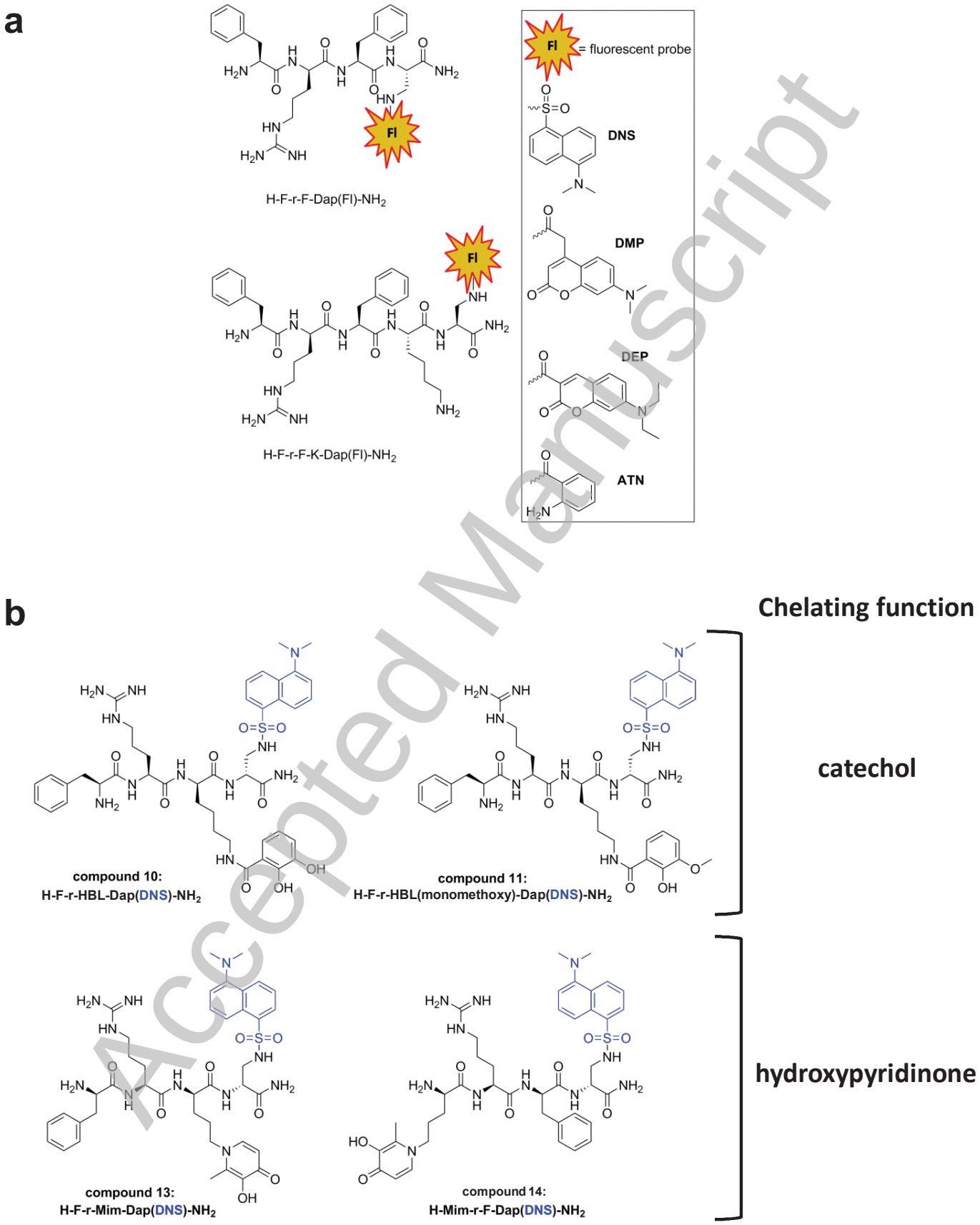

FIGURE 2

a

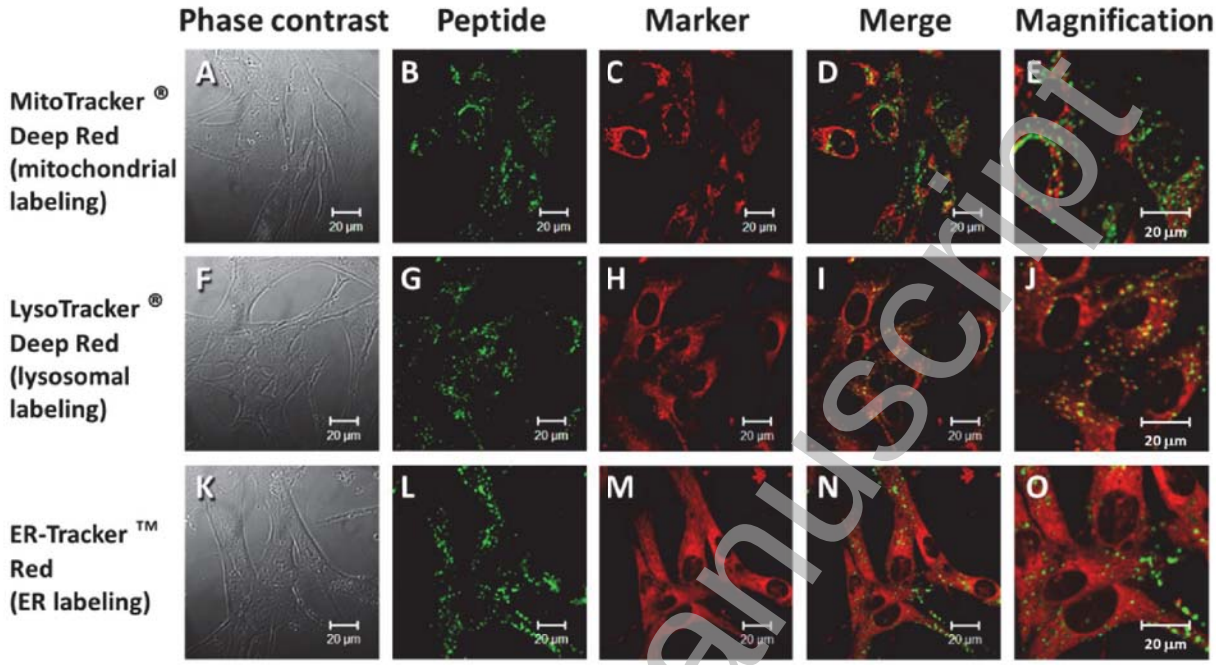

b

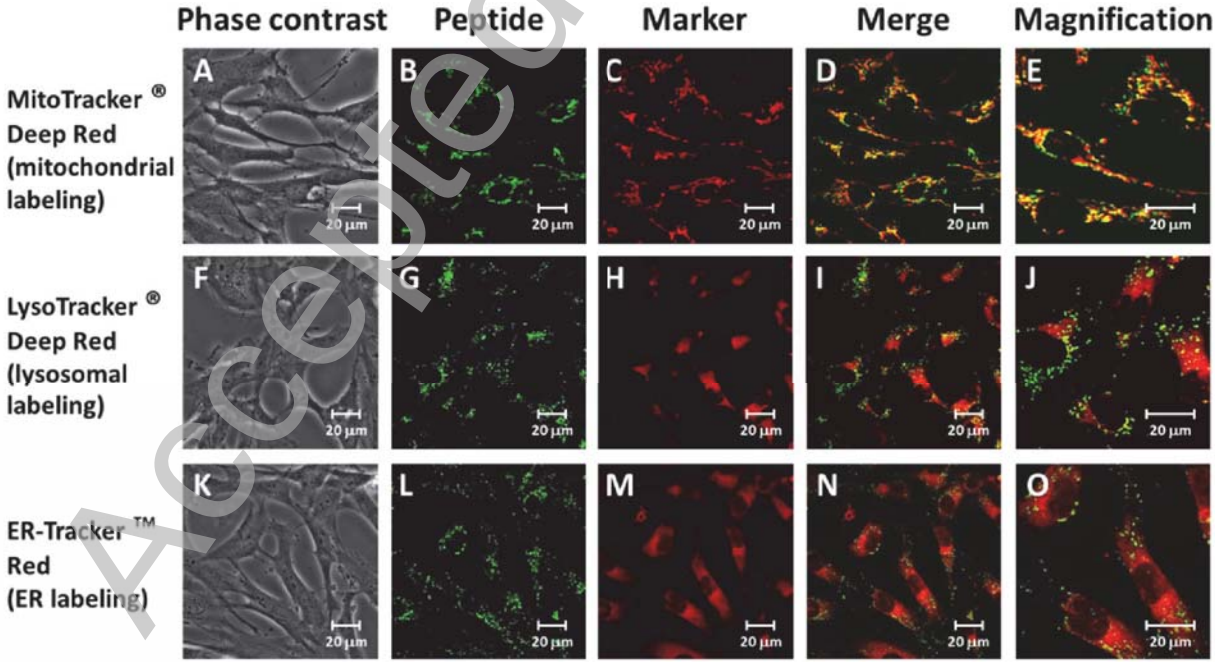

FIG. 3

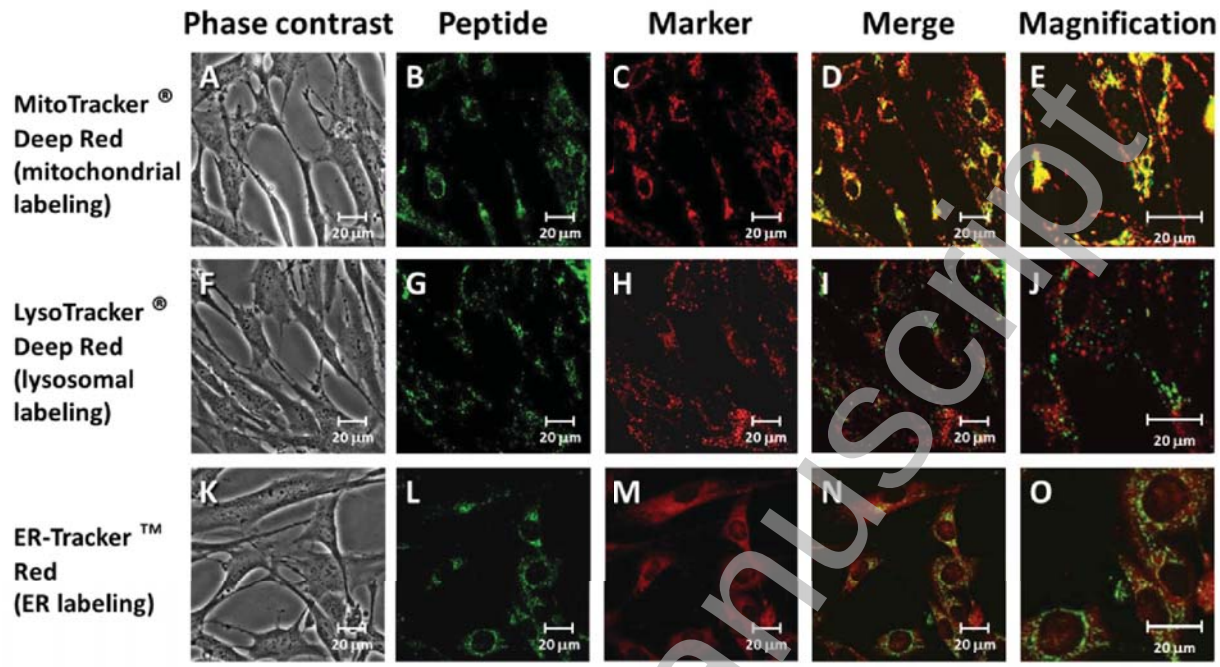

FIG. 4

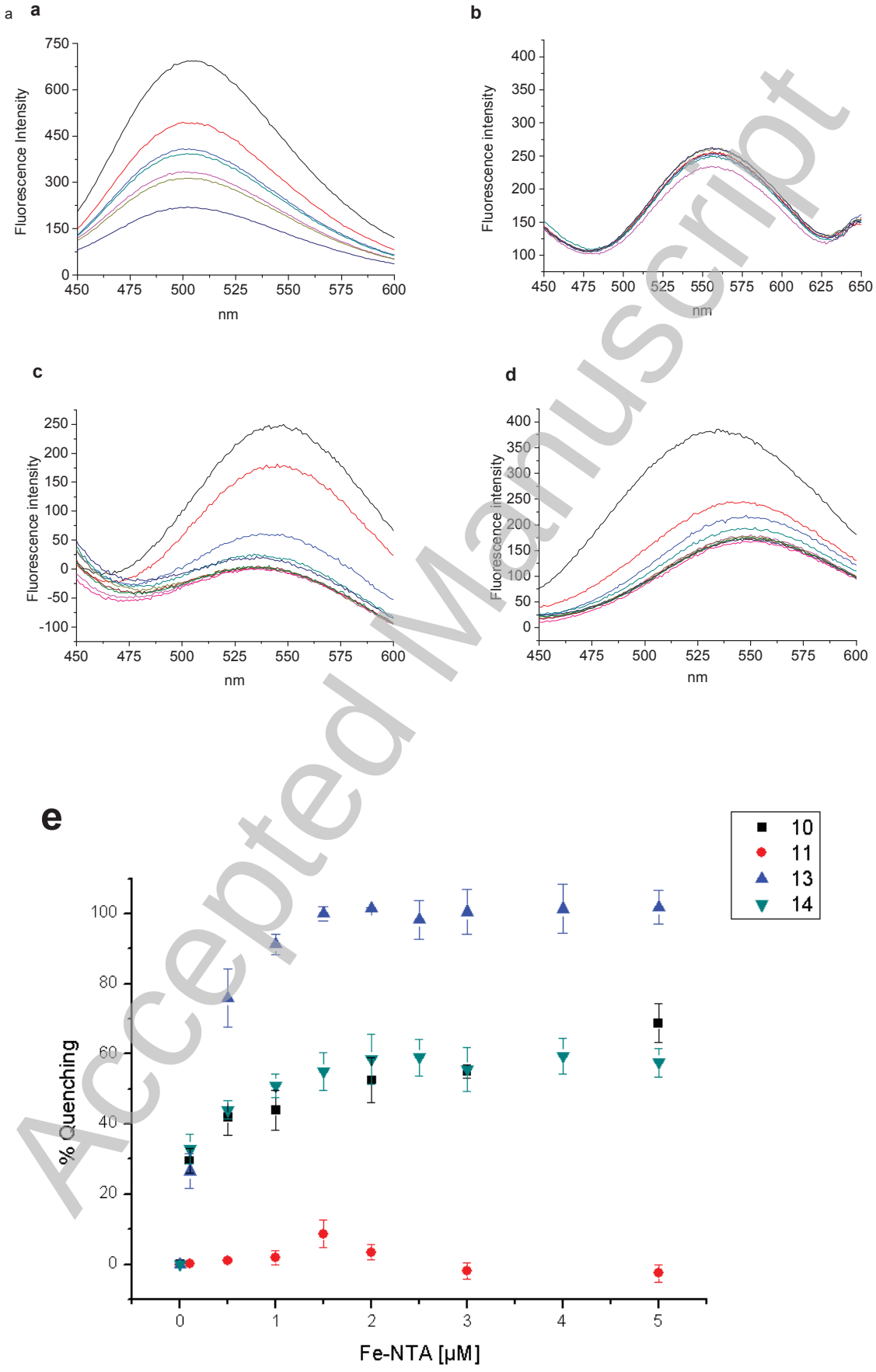

FIGURE 5